

Article

Facile Surfactant-Assisted Synthesis of BiVO₄ Nanoparticulate Films for Solar Water Splitting

Laura Montañés, Camilo A. Mesa , Ana Gutiérrez-Blanco, Christian Robles , Beatriz Julián-López * 
and Sixto Giménez * 

Institute of Advanced Materials (INAM), Universitat Jaume I, Avenida de Vicent Sos Baynat, s/n, 12006 Castellón de la Plana, Spain; lmontane@uji.es (L.M.); cmesa@uji.es (C.A.M.); angutier@uji.es (A.G.-B.); crobles@uji.es (C.R.)

* Correspondence: julian@uji.es (B.J.-L.); sjulia@uji.es (S.G.)

Abstract: Bismuth vanadate (BiVO₄), which has attractive applicability as a photoactive material, presents applications that range from catalysis to water treatment upon visible light irradiation. In this study, we develop a simple synthesis of < 200 nm monoclinic BiVO₄ nanoparticles, which were further deposited on transparent conductive substrates by spin coating and calcination, obtaining nanostructured films. The obtained nanostructured BiVO₄ photoanodes were tested for water oxidation, leading to promising photocurrents exhibiting competitive onset potentials (~0.3 V vs. RHE). These nanoparticulate BiVO₄ photoanodes represent a novel class of highly potential materials for the design of efficient photoelectrochemical devices.



Citation: Montañés, L.; Mesa, C.A.; Gutiérrez-Blanco, A.; Robles, C.; Julián-López, B.; Giménez, S. Facile Surfactant-Assisted Synthesis of BiVO₄ Nanoparticulate Films for Solar Water Splitting. *Catalysts* **2021**, *11*, 1244. <https://doi.org/10.3390/catal11101244>

Academic Editors: María Isabel Díez García, Sebastian Murcia-López and Juan Ramon Morante

Received: 15 September 2021

Accepted: 13 October 2021

Published: 15 October 2021

Publisher's Note: MDPI stays neutral with regard to jurisdictional claims in published maps and institutional affiliations.



Copyright: © 2021 by the authors. Licensee MDPI, Basel, Switzerland. This article is an open access article distributed under the terms and conditions of the Creative Commons Attribution (CC BY) license (<https://creativecommons.org/licenses/by/4.0/>).

Keywords: bismuth vanadate; water splitting; photoanode; nanostructured

1. Introduction

The capture of solar energy and its direct conversion into chemical energy using artificial photosystems is one of the most promising routes to provide the global demand of energy in a sustainable way. Among all the different existing approaches, photoelectrochemical (PEC) energy conversion has attracted a great amount of interest in solar energy storage through the formation of chemical bonds in the form of hydrogen (H₂) or carbon-based fuels [1,2]. These systems are normally based on semiconductor materials, operating as the core of the photoanode and/or photocathode, that absorb solar energy, in a photoelectrochemical cell [3]. After four decades of research on this topic [4], the main challenge still lies in the search for efficient, inexpensive, stable, and scalable semiconductors, particularly as photoanodes, where the oxygen evolution reaction (OER) takes place. Metal oxides and metal oxide anions (oxometalates) are the most studied photoanode materials due to the adequate position of their valence band towards water oxidation as well as their good stability under oxidizing conditions.

In this context, BiVO₄ has attracted much attention due to its low-cost, earth-abundant composition, high chemical and physical stability, and robust and efficient performance as photoanode for water oxidation [5]. This material exhibits three different crystalline structures: tetragonal scheelite, monoclinic scheelite, and tetragonal zircon [6]. Among the different crystal structures, monoclinic BiVO₄ (m-BiVO₄) presents a characteristic relatively narrow bandgap of 2.4 eV, allowing a superior light harvesting efficiency compared to TiO₂ or WO₃ [7], and showing excellent photoelectrocatalytic performance, compared to the other crystal phases. Additionally, monoclinic bismuth vanadate crystals show preferentially exposed {011} facets that exhibit higher surface photovoltage compared to other facets [8]. This behavior strongly suggests that this facet is the most active for photoelectrochemical applications, demonstrating that the crystal orientation plays a key role in the functional performance of the material. As such, it is key to target monoclinic BiVO₄ in the facile synthesis reported in this paper.

The increasing interest in the use of BiVO_4 has led to a large number of studies related to novel synthetic approaches. At present, some of the most common synthetic methods include microwave-assisted [9], co-precipitation [10], hydrothermal, and solid-state reactions [11,12]. Nonetheless, these synthetic processes lead to BiVO_4 structures with irregular shapes, large crystal sizes, and low surface area due to the rapid crystal growth of BiVO_4 [13]. Furthermore, the difficult deposition on conductive substrates limits their applicability as photoelectrodes [14]. The most efficient BiVO_4 photoelectrodes reported to date are grown by electrodeposition [15], metal–organic decomposition [16], spin-coating [17], and spray pyrolysis methods [18,19], but they also present some drawbacks, such as the need for expensive equipment and reagents as well as complicated post-treatments. In particular, compact films are usually achieved by these deposition methods, limiting the obtained photocurrents due to the low exposed surface area. As such, one of the main pathways to increase the photocurrents of photoelectrodes is to increase their surface area per electrode volume by nanostructuring the films and by using BiVO_4 nanoparticles (NPs), as it is performed in the present study. This strategy results in the shortening of the distance that minority charge carriers travel to reach the interface, thus reducing electron–hole recombination [20,21].

To induce nanostructures in photoelectrodes, surfactant molecules can be employed as structure-directing agents during the BiVO_4 synthesis [22]. Surfactants, in polar or nonpolar solvents, are able to organize themselves creating different micellar, lamellar, and other organized structures when the critical micellar concentration is achieved. The organization depends on the nature of the surfactant (i.e., cationic, anionic, or non-ionic). Furthermore, the surfactant shell provides a dynamic solid–liquid interface during the BiVO_4 crystallization process, limiting the fast growth of the nanoparticles. The surfactant-assisted synthesis of monoclinic BiVO_4 nanoparticles has not been extensively investigated. Most studies only address the influence on the particle morphology and its photocatalytic activity, such as the photodegradation of pollutants or dyes. Few studies have been devoted to the formation of monoclinic BiVO_4 nanoparticles assisted by template molecules and/or surfactants, such as ethylene glycol, Pluronic P-123, and Sodium dodecyl sulphate, and their assessment as photoanodes for PEC water splitting. In general, these studies reveal a positive effect, but the materials appeared as agglomerated or irregular polyhedral microcrystals, or even rod-like nanostructures with poor features, to construct homogeneous nanostructured BiVO_4 films [23–27]. Therefore, there is a significant gap in the research to explore the surfactant-assisted synthesis of monoclinic BiVO_4 NPs to design nanoporous photoelectrodes. Note that different deposition techniques, such as doctor blade and aerosol deposition methods, have been previously studied to deposit BiVO_4 nanoparticles in similar configurations [28,29].

For this work, we selected sodium dodecylbenzene sulfonate (SDBS) as anionic surfactant in our synthesis, which has a low critical micellar concentration in water (2.4 mM) and is able to stabilize NPs due to its long aliphatic chain [30,31]. We found that the surfactant does not only acts as a size controller, but also protects the NPs and keeps them separated, avoiding their fast precipitation and aggregation. Consequently, the design of a synthetic procedure through which the nanoparticles are prepared in a combination with a surfactant offers clear advantages, since it allows us to disperse them into organic solvents for their subsequent deposition by techniques, such as spin coating. Furthermore, after light excitation, carriers were photogenerated in BiVO_4 -based photoanode thin films and the diffusion length was directly related to the mobility of these carriers, playing a key role in the porosity of the material to successfully orthogonalize light absorption and carrier diffusion. Indeed, the diffusion length of BiVO_4 was estimated by Abdi and co-researchers as ~70 nm [19].

In this study, we present a novel and simple methodology to obtain BiVO_4 nanoparticles using a SDBS surfactant as a distribution and control size agent. In a different manner to the previously reported synthesis of BiVO_4 , this procedure offers the advantage of using non-expensive precursors in an aqueous medium at a low temperature, resulting in high-

crystallinity monoclinic scheelite BiVO_4 . The mild reaction conditions of this methodology are promising for future up-scalable and continuous flow manufacturing processes. Moreover, for the first time, to the best of our knowledge, we report nanoparticulated BiVO_4 films, which provide a high surface area by a morphological modification of the material.

2. Results and discussion

2.1. Synthesis and Structural Analysis of the BiVO_4 Nanoparticles

The BiVO_4 nanoparticles were synthesized by a modified precipitation process based on a previously reported method (see experimental method in Section 3.1) [23]. The crystalline structure of BiVO_4 was first examined by XRD (Figure 1). The X-ray diffractograms of the as-prepared nanoparticles synthesized with SDBS (SDBS-BiVO_4) (line a in Figure 1), and without surfactant for comparison (BiVO_4) (line b in Figure 1), are consistent with a preferential growth of the monoclinic bismuth vanadate structure [32]. No significant differences on the crystallinity of the monoclinic bismuth vanadate were detected with the incorporation of the surfactant in the synthetic procedure. The average crystallite size was estimated using the Scherrer equation [33] and both samples presented similar values: 29.9 nm and 27.6 nm for SDBS-BiVO_4 and BiVO_4 samples, respectively.

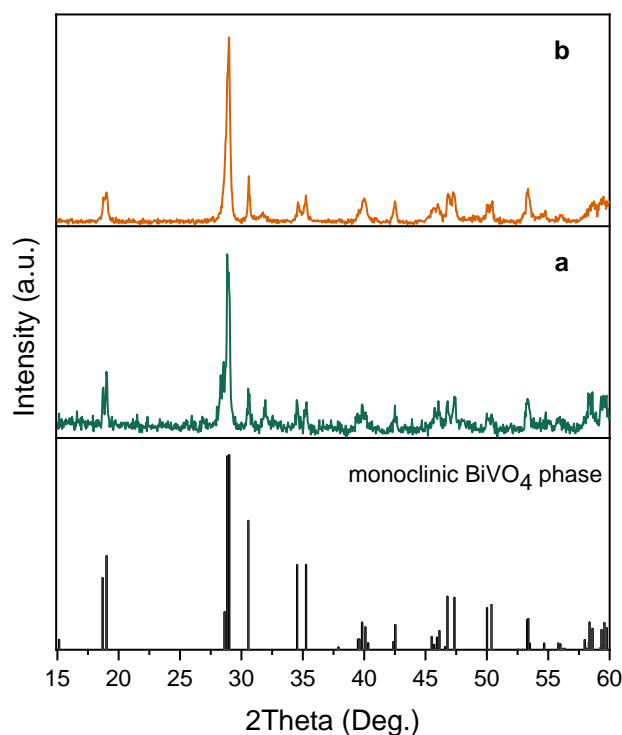


Figure 1. XRD patterns of the calcinated samples: (a) SDBS-BiVO_4 and (b) BiVO_4 , compared to the monoclinic BiVO_4 phase for reference (ICSD 33243 collection code), confirming the preferential growth of the monoclinic BiVO_4 phase by our surfactant-assisted synthesis method.

To study in detail the surface properties of the nanoparticles obtained by surfactant-assisted synthesis, we calculated the surface area available for adsorption of gas molecules by applying the theory of Brunauer, Emmett, and Teller (BET) [34]. The specific surface area of the BiVO_4 was estimated to be $6.8 \text{ m}^2/\text{g}$, based on a fitting analysis using the BET Equation (see the Materials and Methods Section, below, for details). This result is in good agreement with previously reported values between $1\text{--}10 \text{ m}^2/\text{g}$ [35–37].

The morphology of the bismuth vanadate nanoparticles was studied by scanning electron microscopy (SEM). Figure 2a,b demonstrate a clear effect on the morphology of the material achieved by surfactant-assisted synthesis. Without surfactant, irregular-shaped aggregated particles were obtained; meanwhile in the SDBS-BiVO_4 sample, the micrographs

revealed mostly a nanoworm-like structure, with rounded particles of around 80–150 nm. The chelating effect of dodecylbenzene sulphonate anions, which interact electrostatically with BiO^+ species, limited the access of HVO_4^{2-} oxovanadate to form BiVO_4 nuclei. Thus, the nucleation and growth of BiVO_4 crystals in the presence of SDBS was self-limited, providing a nanostructured morphology. The calcination process slightly affected the morphological features, as revealed in Figure 2b,c and only an effect of sintering was detected, leading to the enhanced interconnection of nanoparticles. These SDBS- BiVO_4 nanoparticles were used, to the best of our knowledge, for the first time in this study to produce nanoparticulate photoelectrodes (see Figure 2d for a top view of the film). Such BiVO_4 photoelectrodes preserve their nanoworm-like structure. A heterogeneous distribution of the particles on top of the FTO substrates was detected, probably due to the limited adhesion of the NPs to the substrate. Even though the deposition process can be optimized for a more conformal covering of the substrate, the BiVO_4 film exhibited a good nanostructure, which was the main objective of the present study. Additional SEM images at different magnifications taken with backscattered electron (BSE) and secondary electron (SE) detectors, as well as the energy-dispersive X-ray spectroscopy (EDS) spectrum for the SDBS- BiVO_4 sample, are included as Supplementary Information, Figure S1. The compositional analyses of all the samples made by EDS fit well with the bismuth vanadate stoichiometry.

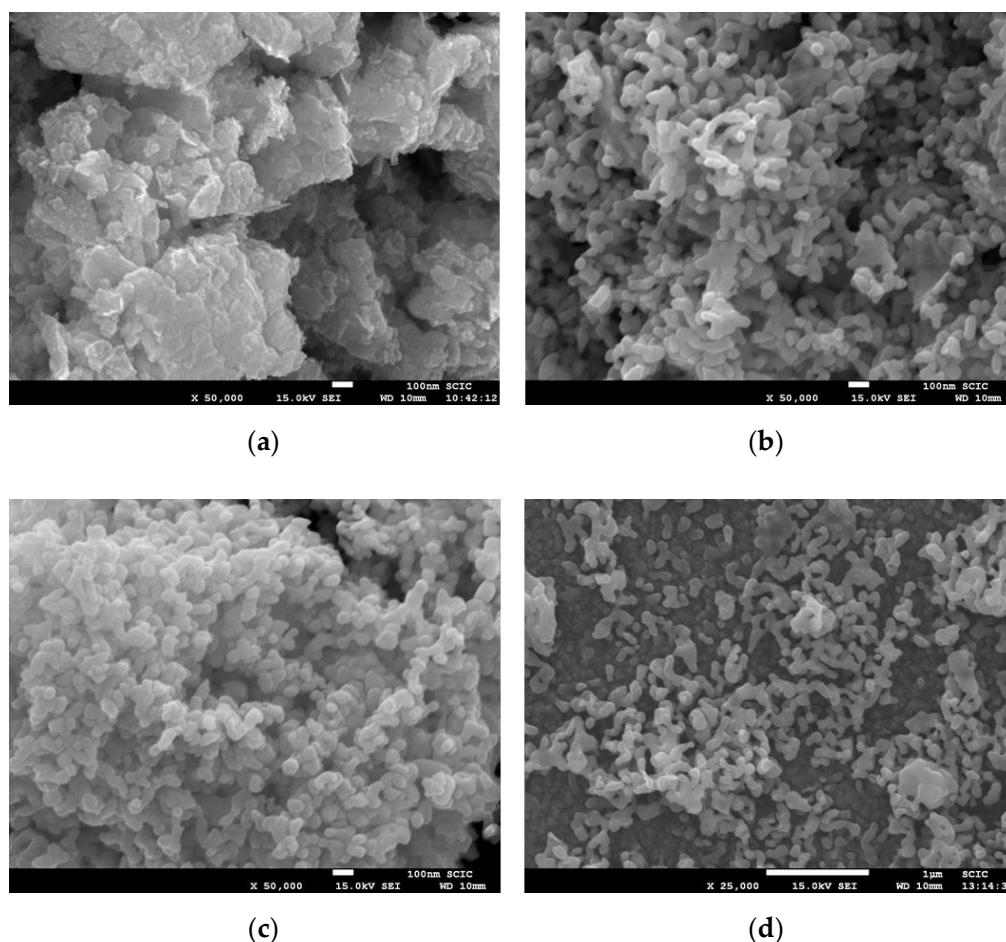


Figure 2. SEM images of (a) calcined BiVO_4 , (b) calcined SDBS- BiVO_4 , (c) SDBS- BiVO_4 before calcination and (d) the top view of a BiVO_4 film (50 layers) after calcination. Scale bars are 100 nm in (a–c) and 1 μm in (d).

Vibrational spectroscopies (such as Raman and Fourier transform infrared (FTIR) spectroscopy) are useful techniques to probe the local structure of the materials. The Raman

spectrum provided important information about the crystalline phase (complementary to XRD) and the coordination of vanadate polyhedra. In particular, the monoclinic-BiVO₄ exhibited some characteristic modes corresponding to the tetrahedral VO₄³⁻ anion. Figure 3a depicts the similar Raman spectra registered for SDBS-BiVO₄ before and after calcination, indicating that the synthetic methodology produces BiVO₄ in the monoclinic phase. The Raman bands located at 826, 720, 368 and 334 are assigned to the shorter symmetric VO stretching mode (A_g), anti-symmetric VO stretching mode (A_g), asymmetric (A_g), and symmetric deformation of tetrahedral VO₄³⁻, respectively, in good agreement with the bands of m-BiVO₄ reported in literature [38]. Two external modes of rotation/translation were also identified at 211 cm⁻¹ and 126 cm⁻¹ [39].

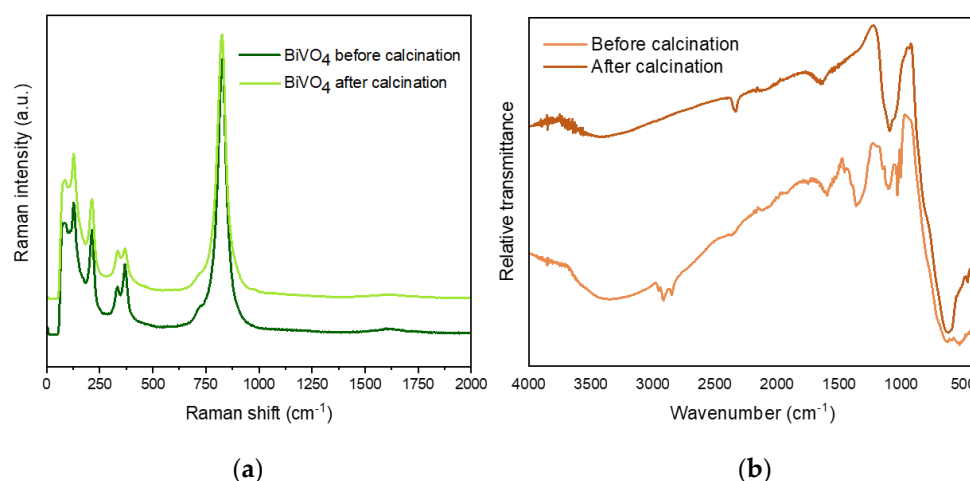


Figure 3. (a) Raman shift and (b) FTIR spectra of the SDBS-BiVO₄ samples before and after calcination.

The FTIR vibrational spectra are also included in Figure 3b. The broad and strong FTIR band centered at 720 cm⁻¹ with shoulders around at 690, 810, and 890 cm⁻¹ corresponds to the stretching modes of tetrahedral VO₄³⁻, and it was observed both before and after calcination on BiVO₄ samples [40]. The bands appearing at ~1640 cm⁻¹ and above 3000 cm⁻¹ correspond to H₂O molecules adsorbed on the surface of the material [11], and they are also visible in both spectra. Interestingly, before calcination, some fingerprints from SDBS were detected: the signals at 1049 cm⁻¹ and 1151 cm⁻¹ correspond to the symmetric and asymmetric stretching, respectively, of sulfonic acid group [41], and the stretching modes from CH skeleton at around 2900 cm⁻¹. This latter band disappeared upon calcination indicating the non-existence of carbon chemical residues after this process. However, some residual SO₃⁻ was still detected, which could be adsorbed on the surface of the NPs.

2.2. Preparation of BiVO₄ Films and Optical Characterization

After the synthesis of the SDBS-BiVO₄ nanoparticles, BiVO₄ films were prepared by spin-coating (represented in Figure 4) and further characterized and tested for the water oxidation reaction. UV-vis spectroscopy is the most common method used to characterize the bandgaps of semiconductors. Efficient light absorption is an essential feature to consider in photoelectrochemical activity of photoelectrodes [42]. Therefore, absorption spectra were recorded for the films with different thicknesses (Figure 5a), showing the typical optical fingerprint for this semiconductor at wavelengths shorter than ~500 nm. The direct bandgap was also calculated from their respective Tauc plots. It is apparent from Figure 5b that the direct bandgap (E_g) of our m-BiVO₄ films (50 layers) is 2.46 eV which is consistent with the 2.4 eV reported in the literature for m-BiVO₄ [43]. Similar results were obtained for 10 and 20 layers, as shown in the Supplementary Information (Figure S2).

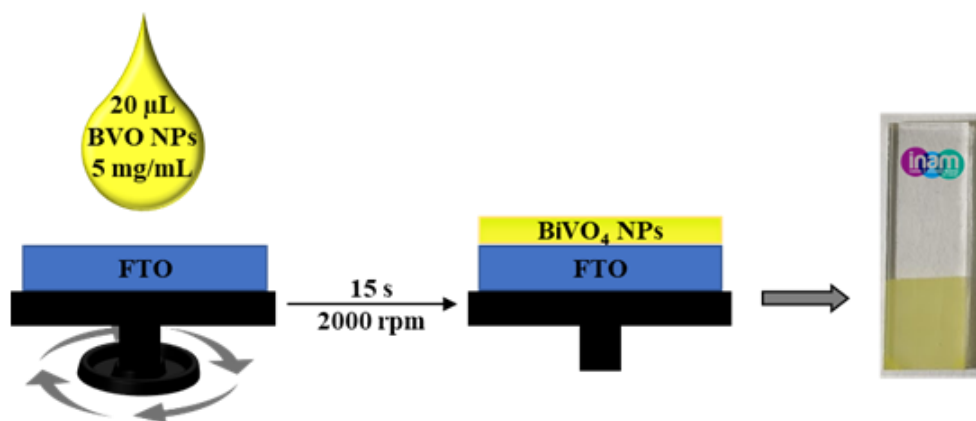


Figure 4. Scheme of nanoparticle deposition by the spin coating technique and image of the obtained photoelectrode after calcination.

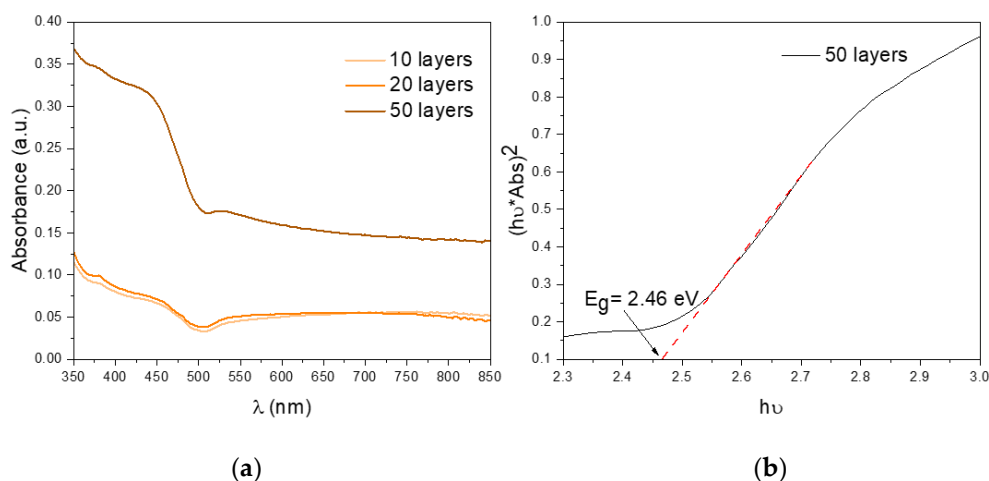


Figure 5. (a) UV-vis spectra of the 10 (light orange), 20 (orange) and 50 (brown) layer films and (b) Tauc plot for band-gap determination.

2.3. Photoelectrochemical Characterization

The photoelectrochemical properties of the photoelectrodes were evaluated in the presence of a hole scavenger (Na_2SO_3). A considerable photocurrent increase upon calcination is shown in Figure 6a. A tenfold photocurrent increase was observed after removing the SDBS surfactant and forming the nanoworms, reaching a photocurrent of $\sim 130 \mu\text{A cm}^{-2}$. This photocurrent increase can be attributed to the enhanced intimate contact between the nanoparticles after calcination observed in Figure 2d. Additionally, an improvement of the photocurrent density was noticed as the BiVO_4 layers increase, i.e., larger film thickness (see Figure 6b). Also, the onset potential was found shift to a more negative potential when the number of deposited layers increases. This onset potential (0.33 V vs. RHE) is close to the reported state-of-art values (around 0.2 V vs. RHE) for electrodeposited BiVO_4 photoanodes [44]. This change in the onset potential represents a lower requirement of energy input in PEC water splitting reaction. The complete set of PEC characterization is shown in the Supplementary Information (Figure S3). To understand the nature of the improvement of PEC performance with the increase in the number of layers towards the water oxidation reaction, the electrochemical properties of each photoanode were determined by electrochemical impedance spectroscopy (EIS). Nyquist plots of the 3 BiVO_4 films are shown in Figure 6c in the dark at 0.6 V vs. RHE. Similar results were obtained at other anodic potentials between 0.5–1 V vs. RHE, compiled as Supplementary Information (Figure S4). While the number of layers increased, the arc radius decreased, suggesting an improvement on the charge transfer kinetics of the photoanodes, which is correlated to the

increase on the photogenerated current. Furthermore, the stability of the films synthesized was investigated. Figure 6d shows a chronoamperometric measurement, for an hour, at 1.23 V versus RHE under constant illumination for the film formed by 50 layers presenting a notable stability.

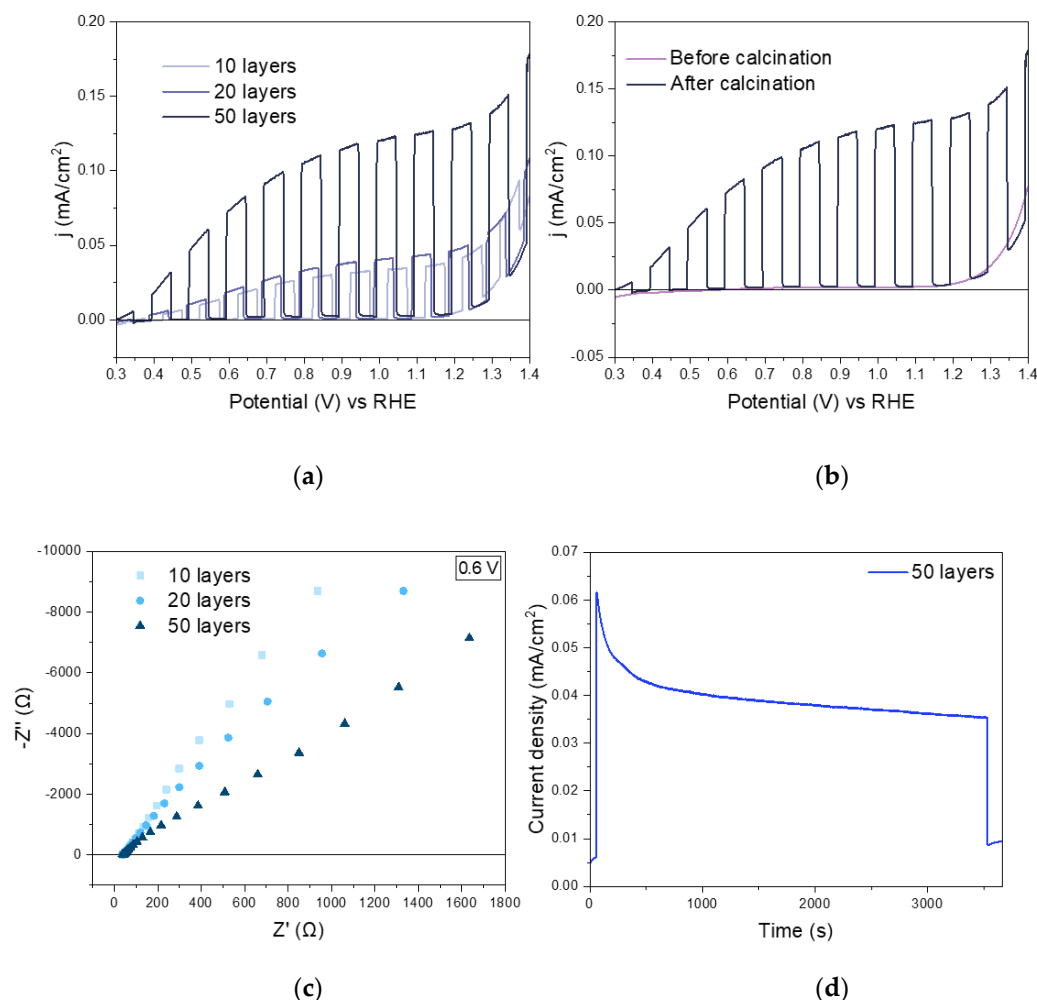


Figure 6. Photoelectrochemical characterization of BiVO₄ in 0.1 M potassium phosphate (KPi) buffer containing 0.1 M sodium sulfite. (a) LSV (linear sweep voltammetry) plot under chopped light BiVO₄ before and after calcination of the SDBS-BiVO₄ (50 layers) photoanode; (b) LSV plots under chopped light of BiVO₄ photoanode with 10, 20 and 50 layers; (c) Nyquist plots of the BiVO₄ photoanode with different thicknesses and (d) chronoamperometry at 1.23 V vs. RHE of BiVO₄ (50 layers).

Note that the films with 10 and 20 layers exhibit a remarkably similar photoelectrochemical response (Figure 6b). This is most likely due to their light absorption properties as shown in Figure 5a, where almost identical UV-Vis spectra are shown. To explain the similar performance of the films containing 10 and 20 layers of BiVO₄, the electrochemical active surface area (ECSA) of the samples was calculated by using electrochemical impedance spectroscopy (EIS) in the non-faradaic region, by the following equation:

$$ECSA = \frac{C_{DL}}{C_s} \quad (1)$$

where C_{DL} corresponds to the electrochemical double layer capacitance, which was determined by the frequency-dependent complex impedance at low frequencies [45]. A specific electrochemical double layer capacitance of atomically plane interface (C_s) of 40 μF cm⁻² was used according to previously reported values [46,47].

The calculated ECSA were 0.44, 0.45 and 0.53 cm² for 10, 20, and 50 layers in the BiVO₄ photoanodes, respectively. The ECSA values for the films with 10 and 20 layers were almost identical and nicely correlate with the optical response as well as with the photoelectrochemical performance. The higher ECSA value, which corresponds to the sample of 50 layers, supports the critical influence of the active surface region on the photoelectrochemical activities. Note that, in general, the low ECSA response indicates that it is possible to increase the photoresponse by improving the deposition of the nanoparticles.

3. Materials and Methods

All the reagents and solvents were used as received from commercial suppliers (Bi(NO₃)₃·5H₂O, V₂O₅, SDBS, NaOH, Na₂SO₃, KH₂PO₄, K₂HPO₄ and toluene) and without further purification. Milli-Q water was used to prepare all solutions. Bismuth vanadate was synthesized by the direct precipitation of vanadate and bismuth precursor aqueous solutions in the presence of SDBS.

3.1. Synthesis of BiVO₄ Nanoparticles

In a typical synthesis, 0.2501 mmol (0.1213 g) of Bi(NO₃)₃·5H₂O were dissolved in 25 mL of a 2.28 mM SDBS aqueous solution, named as solution A. Simultaneously, 0.1251 mmol (23.22 mg) of V₂O₅ and 0.7503 mmol of NaOH (15.57 mg) were dissolved in 25 mL of Milli-Q water, named as solution B. Both solutions were stirred at 35 °C for 30 min. Then, solution B was added drop by drop to solution A and a yellow suspension was formed. After stirring for an hour at 35 °C, the precipitate was recovered by centrifugation (10000 rpm for 5 min), and washed once with distilled water and once with ethanol. The yellow powder was dried at 60 °C overnight. The sample (SDBS-BiVO₄) was calcinated at 500 °C for 2 h in air (ramping rate = 2 °C min⁻¹) to increase the crystallinity and eliminate the surfactant, and the product exhibited a vivid yellow color. A reference sample of BiVO₄ without adding SBDS was also prepared following the same procedure, for comparison purposes.

3.2. Preparation of the Nanostructured BiVO₄ Films

First, FTO substrates were washed ultrasonically in soap water, Milli-Q water and in a mixture of acetone/isopropanol (1:3) each for 14 min and dried in an oven. Subsequently, rinsed FTO substrates were cleaned using a UV-ozone chamber. A 5 mg/mL of the SDBS-BiVO₄ colloidal solution was prepared by dispersing the nanoparticles in toluene and ultrasonicated for 30 min. To make thin films, the spin coating technique was used. An amount of 20 µL of the colloidal suspension were deposited on FTO substrates at 1500 rpm every 15 s for each repetition. Several repetitions (10, 15, 20, 50, and 75 layers) were made by spin-coating to study the influence of the thickness on the electrode photoactivity. The resulting films were calcined at 500 °C for 2 h in air (ramping rate = 2 °C min⁻¹) to obtain nanostructured BiVO₄ films. This calcination allows the removal of the surfactants and the generation of porosity in the photoelectrodes.

3.3. Structural and Morphology Characterization of the BiVO₄ Nanoparticles

An X-ray diffractometer with a Cu K α radiation ($\lambda = 1.5418 \text{ \AA}$) operating at a grazing incidence of 1°, and at a scan speed of 3° min⁻¹ for 2 θ angles from 15 to 70° was used to obtain X-ray diffraction (XRD) patterns of the samples. The morphology and composition of the BiVO₄ nanoparticles were examined by field-emission scanning electron microscopy (FE-SEM) with a JSM-700F JEOL FEG-SEM system (Tokyo, Japan) equipped with an INCA 400 Oxford EDS analyzer (Oxford, UK.) operating at 15 kV. Before the FE-SEM experiment, the samples were sputtered with a 2 nm thick layer of Pt. Raman spectroscopy was carried out with a WITec Apyron confocal microscope using a 532 nm laser with a 1 mW power, a grating of 1800 g/mm, a BLZ = 500 nm and an optical objective Zeiss EC Epiplan-Neofluar Dic 50x/0.55. The surface area of the BiVO₄ was determined by measuring nitrogen adsorption-desorption isotherms at liquid nitrogen temperature (77 K) using a surface area

analyzer (Micromeritics' TriStar 3000) equipped with a FlowPrep 060. The sample was degassed at 150 °C during 2 h under vacuum before the adsorption measurements. The specific surface was calculated following the BET method from the adsorption isotherm using the equation:

$$S_{BET} \left(m^2 g^{-1} \right) = n_m a_{nitrogen} N_A \quad (2)$$

where n_m is the gas capacity in the monolayer that covers the material surface; $a_{nitrogen}$ ($a_{nitrogen} = 0.162 \text{ nm}^2$) is the transversal section of the nitrogen molecule and N_A is the Avogadro number. The results of the analysis are collected in Table S1.

3.4. Optical and Photoelectrochemical Characterization of the BiVO₄ Photoanodes

The optical response of the spin-coated BiVO₄ photoanodes was recorded on a Lambda 1050+ spectrophotometer (Perkin Elmer) using BaSO₄ as reference for the diffuse reflectance. The absorbance (A) was estimated by $A = -\log(T + R)$, where T is transmittance and R corresponds to the diffuse reflectance. The direct optical bandgap could be estimated by the Tauc plot as $(h\nu\alpha)^2 = A(h\nu - E_g)$, where E_g is the band gap, $h\nu$ is the photon energy and A is a proportionality constant.

The photoelectrochemical properties of the photoelectrodes were obtained using an Autolab potentiostat/galvanostat PGSTAT302, and the light source was a 300 W Xe lamp with AM 1.5 G, adjusting the light intensity to 100 mW cm⁻² using a Si photodiode. Cyclic voltammetry (CV) and linear sweep voltammetry with a scan rate of 10 mV s⁻¹ in the dark and under illumination were carried out at room temperature in a home-made three-electrode cell with the photoanode, Pt coil and Ag/AgCl as a working, counter, and reference electrodes, respectively. The electrolyte was a 0.1 M potassium phosphate (KPi) buffer aqueous solution (pH 7.0) with 0.1 M Na₂SO₃ serving as a hole scavenger. Since the potential was measured against Ag/AgCl, all the potential measurements were converted to the reversible hydrogen electrode (RHE) by using the Nernst equation:

$$E_{RHE} = E_{Ag/AgCl} + E_{Ag/AgCl}^0 + 0.0591V * pH$$

$$\left(E_{Ag/AgCl}^0 = 0.1976V \text{ vs. NHE at } 25^\circ C \right) \quad (3)$$

4. Conclusions

In conclusion, we have reported, to the best of our knowledge, the fabrication of nanostructured BiVO₄ photoanodes by spin-coating of BiVO₄ nanoparticles for the first time. In the present study, we also demonstrate an easy method to prepare BiVO₄ nanoparticles via an aqueous low temperature (35 °C) surfactant-assisted synthetic procedure. The SDBS surfactant provided a good control in the morphology of nanocrystals, obtaining particle sizes appropriated to enhance charge separation, without affecting the crystallization of the monoclinic phase. Nanostructuring of BiVO₄ was demonstrated to display a positive effect on the functional performance of photoelectrodes. However, although the photocurrents reported upon irradiation in this work did not present a high performance we would like to emphasize that these films are the first nanoparticulate ones reported to date without the employment of doping or further heterostructuring strategies, which opens the door to a new route of producing high surface area BiVO₄ photoanodes. Consequently, we believe that this study could open new avenues in the synthesis of efficient photoelectrodes with applicability in different fields.

Supplementary Materials: The following are available online at <https://www.mdpi.com/article/10.3390/catal11101244/s1>: Figure S1: SEM images of the BiVO₄ sample before calcination taken with (a) secondary electron detector (SEI) and (b) backscattered electron detector (COMPO); (c) COMPO micrograph from the SDBS-BiVO₄ sample before calcination; (d) representative EDS spectrum of the SDBS-BiVO₄ sample. Figure S2: Tauc plots for bandgap determination: (a) 10 layers (b), 20 layers (c), and 50 layers before calcination. Figure S3: Cyclic voltammeteries of BiVO₄ in 0.1 M KPi buffer containing 0.1 M sodium sulfite of (a) 50 layers before calcination and (b) 10 layers, (c) 20 layers, and (d) 50 layers after calcination. Figure S4: Nyquist plots of the BiVO₄ photoanodes with differently thicknesses at different applied potentials: (a) 0.5 V vs. RHE, (b) 0.6 V vs. RHE, (c) 0.7 V vs. RHE, (d) 0.8 V vs. RHE, (e) 0.9 V vs. RHE, and (f) 1 V vs. RHE, Figure S5: Chronoamperometries under illumination at 1.23 V vs. RHE of the BiVO₄ films formed by: (a) 10 layers and (b) 20 layers. Table S1: BET analysis results of BiVO₄ calcinated (obtained by surfactant-assisted synthesis).

Author Contributions: Conceptualization, B.J.-L. and S.G.; investigation, L.M., C.A.M. and C.R.; data curation, L.M., C.A.M., A.G.-B., and C.R.; writing—original draft preparation, L.M., A.G.-B. and C.R.; writing—review and editing, C.A.M., B.J.-L., and S.G.; supervision, B.J.-L. and S.G.; project administration, S.G.; funding acquisition, S.G. All authors have read and agreed to the published version of the manuscript.

Funding: This research was funded by European Commission with the project “SUN2CHEM”, through the Grant Agreement 884444.

Data Availability Statement: Raw data were generated at University Jaume I. Derived data supporting the findings of this study are available from the corresponding authors [B.J.-L. and S.G.] upon request.

Acknowledgments: We gratefully acknowledge the financial support from the European Commission associated to the European project “SUN2CHEM”, through the Grant Agreement 884444. C.A.M., B.J.-L., C.P. and S.G. acknowledge the University Jaume I, for the postdoctoral fellowship POSDOC/2019/20 and projects UJI-B2018-71 and UJI-B2020-50, respectively. We are also grateful to the Serveis Centrals d’Instrumentació Científica from the University Jaume I (SCIC-UJI) for providing all the characterization facilities.

Conflicts of Interest: The authors declare no conflict of interest. The funders had no role in the design of the study; in the collection, analyses, or interpretation of the data; in the writing of the manuscript, or in the decision to publish the results.

References

1. Chen, X.; Zhang, Z.; Chi, L.; Nair, A.K.; Shangguan, W.; Jiang, Z. Recent advances in visible-light-driven photoelectrochemical water splitting: Catalyst nanostructures and reaction systems. *Nano-Micro Lett.* **2016**, *8*, 1–12. [[CrossRef](#)]
2. Lewis, N.S.; Nocera, D.G. Powering the Planet: Chemical Challenges in Solar Energy Utilization. *Proc. Natl. Acad. Sci.* **2006**, *103*, 15729–15735. [[CrossRef](#)]
3. Soni, D.; Parsoya, P.; Menariya, B.K.; Vyas, R.; Ameta, R. Photoelectrochemical cells. *Sol. Energy Convers. Storage Photochem. Modes* **2015**, *414*, 29–53. [[CrossRef](#)]
4. Fujishima, A.; Honda, K. Electrochemical Photolysis of water at a semiconductor electrode. *Nature* **1972**, *238*, 37–38. [[CrossRef](#)] [[PubMed](#)]
5. Park, Y.; Mc Donald, K.J.; Choi, K.S. Progress in bismuth vanadate photoanodes for use in solar water oxidation. *Chem. Soc. Rev.* **2013**, *42*, 2321–2337. [[CrossRef](#)] [[PubMed](#)]
6. Roth, R.S.; Waring, J.L. Synthesis And Stability Of Bismutotantalite, Stibiotantalite And Chemically Similar AB₄ Compounds. *Am. Mineral.* **1963**, *48*, 1348–1356.
7. Kim, J.H.; Lee, J.S. Elaborately Modified BiVO₄ Photoanodes for Solar Water Splitting. *Adv. Mater.* **2019**, *31*, 1806938. [[CrossRef](#)]
8. Zhu, J.; Fan, F.; Chen, R.; An, H.; Feng, Z.; Li, C. Direct Imaging of Highly Anisotropic Photogenerated Charge Separations on Different Facets of a Single BiVO₄ Photocatalyst. *Angew. Chemie Int. Ed.* **2015**, *54*, 9111–9114. [[CrossRef](#)]
9. Zhang, H.M.; Liu, J.B.; Wang, H.; Zhang, W.X.; Yan, H. Rapid microwave-assisted synthesis of phase controlled BiVO₄ nanocrystals and research on photocatalytic properties under visible light irradiation. *J. Nanoparticle Res.* **2008**, *10*, 767–774. [[CrossRef](#)]
10. Yu, J.; Zhang, Y.; Kudo, A. Synthesis and photocatalytic performances of BiVO₄ by ammonia co-precipitation process. *J. Solid State Chem.* **2009**, *182*, 223–228. [[CrossRef](#)]
11. Gotić, M.; Musić, S.; Ivanda, M.; Šoufek, M.; Popović, S. Synthesis and characterisation of bismuth(III) vanadate. *J. Mol. Struct.* **2005**, *744–747*, 535–540. [[CrossRef](#)]
12. Khademinia, S.; Behzad, M.; Jahromi, H.S. Solid state synthesis, characterization, optical properties and cooperative catalytic performance of bismuth vanadate nanocatalyst for Biginelli reactions. *RSC Adv.* **2015**, *5*, 24313–24318. [[CrossRef](#)]

13. Tokunaga, S.; Kato, H.; Kudo, A. Selective preparation of monoclinic and tetragonal BiVO₄ with scheelite structure and their photocatalytic properties. *Chem. Mater.* **2001**, *13*, 4624–4628. [[CrossRef](#)]
14. Tan, H.L.; Amal, R.; Ng, Y.H. Exploring the Different Roles of Particle Size in Photoelectrochemical and Photocatalytic Water Oxidation on BiVO₄. *ACS Appl. Mater. Interfaces* **2016**, *8*, 28607–28614. [[CrossRef](#)] [[PubMed](#)]
15. Lee, D.K.; Lee, D.; Lumley, M.A.; Choi, K.S. Progress on ternary oxide-based photoanodes for use in photoelectrochemical cells for solar water splitting. *Chem. Soc. Rev.* **2019**, *48*, 2126–2157. [[CrossRef](#)] [[PubMed](#)]
16. Sayama, K.; Nomura, A.; Arai, T.; Sugita, T.; Abe, R.; Yanagida, M.; Oi, T.; Iwasaki, Y.; Abe, Y.; Sugihara, H. Photoelectrochemical decomposition of water into H₂ and O₂ on porous BiVO₄ thin-film electrodes under visible light and significant effect of Ag Ion treatment. *J. Phys. Chem. B* **2006**, *110*, 11352–11360. [[CrossRef](#)]
17. Toma, F.M.; Cooper, J.K.; Kunzelmann, V.; McDowell, M.T.; Yu, J.; Larson, D.M.; Borys, N.J.; Abelyan, C.; Beeman, J.W.; Yu, K.M.; et al. Mechanistic insights into chemical and photochemical transformations of bismuth vanadate photoanodes. *Nat. Commun.* **2016**, *7*, 1–11. [[CrossRef](#)] [[PubMed](#)]
18. Su, J.; Guo, L.; Bao, N.; Grimes, C.A. Nanostructured WO₃/BiVO₄ heterojunction films for efficient photoelectrochemical water splitting. *Nano Lett.* **2011**, *11*, 1928–1933. [[CrossRef](#)]
19. Abdi, F.F.; Savenije, T.J.; May, M.M.; Dam, B.; van de Krol, R. The origin of slow carrier transport in BiVO₄ thin film photoanodes: A time-resolved microwave conductivity study. *J. Phys. Chem. Lett.* **2013**, *4*, 2752–2757. [[CrossRef](#)]
20. Berglund, S.P.; Flaherty, D.W.; Hahn, N.T.; Bard, A.J.; Mullins, C.B. Photoelectrochemical oxidation of water using nanostructured BiVO₄ films. *J. Phys. Chem. C* **2011**, *115*, 3794–3802. [[CrossRef](#)]
21. Cowan, A.J.; Durrant, J.R. Long-lived charge separated states in nanostructured semiconductor photoelectrodes for the production of solar fuels. *Chem. Soc. Rev.* **2013**, *42*, 2281–2293. [[CrossRef](#)] [[PubMed](#)]
22. Yin, Y.; Alivisatos, A.P. Colloidal nanocrystal synthesis and the organic-inorganic interface. *Nature* **2005**, *437*, 664–670. [[CrossRef](#)]
23. Zhang, L.; Gonçalves, A.A.S.; Jiang, B.; Jaroniec, M. A generalized strategy for synthesizing crystalline bismuth-containing nanomaterials. *Nanoscale* **2020**, *12*, 8277–8284. [[CrossRef](#)] [[PubMed](#)]
24. Helal, A.; El-Sheikh, S.M.; Yu, J.; Eid, A.I.; El-Haka, S.A.; Samra, S.E. Novel synthesis of BiVO₄ using homogeneous precipitation and its enhanced photocatalytic activity. *J. Nanoparticle Res.* **2020**, *22*. [[CrossRef](#)]
25. Jiang, H.; Dai, H.; Meng, X.; Zhang, L.; Deng, J.; Ji, K. Morphology-dependent photocatalytic performance of monoclinic BiVO₄ for methyl orange degradation under visible-light irradiation. *Cuihua Xuebao/Chinese J. Catal.* **2011**, *32*, 939–949. [[CrossRef](#)]
26. Wang, X.; Li, G.; Ding, J.; Peng, H.; Chen, K. Facile synthesis and photocatalytic activity of monoclinic BiVO₄ micro/nanostructures with controllable morphologies. *Mater. Res. Bull.* **2012**, *47*, 3814–3818. [[CrossRef](#)]
27. García-Pérez, U.M.; Sepúlveda-Guzmán, S.; Martínez- de la Cruz, A.; Peral, J. Selective synthesis of monoclinic bismuth vanadate powders by surfactant-assisted co-precipitation method: Study of their electrochemical and photocatalytic properties. *Int. J. Electrochem. Sci.* **2012**, *7*, 9622–9632.
28. Long, M.; Cai, W. Photoelectrochemical Properties of BiVO₄ Film Electrode in Alkaline Solution. *Chinese J. Catal.* **2008**, *29*, 881–883. [[CrossRef](#)]
29. Wolpert, C.; Emmeler, T.; Villa Vidaller, M.; Elsenberg, A.; Shinoda, K.; Schieda, M.; Gärtner, F.; Akedo, J.; Klassen, T. Aerosol-Deposited BiVO₄ Photoelectrodes for Hydrogen Generation. *J. Therm. Spray Technol.* **2021**, *30*, 603–616. [[CrossRef](#)]
30. Graciaa, A.; Ben Ghoulam, M.; Marion, G.; Lachaise, J. Critical concentrations and compositions of mixed micelles of sodium dodecylbenzenesulfonate, tetradecyltrimethylammonium bromide, and polyoxyethylene octylphenols. *J. Phys. Chem.* **1989**, *93*, 4167–4173. [[CrossRef](#)]
31. Su, Y.L.; Liu, H.Z. Temperature-dependent solubilization of PEO-PPO-PEO block copolymers and their application for extraction trace organics from aqueous solutions. *Korean J. Chem. Eng.* **2003**, *20*, 343–346. [[CrossRef](#)]
32. Sleight, A.W.; Chen, H.Y.; Ferretti, A.; Cox, D.E. Crystal growth and structure of BiVO₄. *Mater. Res. Bull.* **1979**, *14*, 1571–1581. [[CrossRef](#)]
33. Patterson, A.L. The scherrer formula for X-ray particle size determination. *Phys. Rev.* **1939**, *56*, 978–982. [[CrossRef](#)]
34. Brunauer, S.; Emmett, P.H.; Teller, E. Adsorption of Gases in Multimolecular. *J. Am. Chem. Soc.* **1938**, *60*, 309–319. [[CrossRef](#)]
35. Hu, J.; Zhai, C.; Zeng, L.; Du, Y.; Zhu, M. Enhanced electrocatalytic ethanol oxidation reaction in alkaline media over Pt on a 2D BiVO₄-modified electrode under visible light irradiation. *Catal. Sci. Technol.* **2018**, *8*, 3562–3571. [[CrossRef](#)]
36. Bommineedi, L.K.; Pandit, B.; Sankapal, B.R. Spongy nano surface architecture of chemically grown BiVO₄: High-capacitance retentive electrochemical supercapacitor. *Int. J. Hydrogen Energy* **2021**, *46*, 25586–25595. [[CrossRef](#)]
37. Dolić, S.D.; Jovanović, D.J.; Smits, K.; Babić, B.; Marinović-Cincović, M.; Porobić, S.; Dramićanin, M.D. A comparative study of photocatalytically active nanocrystalline tetragonal zircon-type and monoclinic scheelite-type bismuth vanadate. *Ceram. Int.* **2018**, *44*, 17953–17961. [[CrossRef](#)]
38. Galembeck, A.; Alves, O.L. BiVO₄ thin film preparation by metalorganic decomposition. *Thin Solid Films* **2000**, *365*, 90–93. [[CrossRef](#)]
39. Hardcastle, F.D.; Wachs, I.E. Determination of vanadium-oxygen bond distances and bond orders by Raman spectroscopy. *J. Phys. Chem.* **2002**, *95*, 5031–5041. [[CrossRef](#)]
40. Liu, J.B.; Wang, H.; Wang, S.; Yan, H. Hydrothermal preparation of BiVO₄ powders. *Mater. Sci. Eng. B Solid-State Mater. Adv. Technol.* **2003**, *104*, 36–39. [[CrossRef](#)]

41. Shukla, A.; Bhat, S.D.; Pillai, V.K. Simultaneous unzipping and sulfonation of multi-walled carbon nanotubes to sulfonated graphene nanoribbons for nanocomposite membranes in polymer electrolyte fuel cells. *J. Memb. Sci.* **2016**, *520*, 657–670. [[CrossRef](#)]
42. Tauc, J.; Grigorovici, R.; Vanacu, A. Optical Properties and Electronic Structure of Amorphous Germanium. *Phys. Stat. Sol.* **1966**, *1*, 627–637. [[CrossRef](#)]
43. Kudo, A.; Omori, K.; Kato, H. A novel aqueous process for preparation of crystal form-controlled and highly crystalline BiVO₄ powder from layered vanadates at room temperature and its photocatalytic and photophysical properties. *J. Am. Chem. Soc.* **1999**, *121*, 11459–11467. [[CrossRef](#)]
44. Lee, D.K.; Choi, K.S. Enhancing long-term photostability of BiVO₄ photoanodes for solar water splitting by tuning electrolyte composition. *Nat. Energy* **2018**, *3*, 53–60. [[CrossRef](#)]
45. McCrory, C.C.L.; Jung, S.; Ferrer, I.M.; Chatman, S.M.; Peters, J.C.; Jaramillo, T.F. Benchmarking Hydrogen Evolving Reaction and Oxygen Evolving Reaction Electrocatalysts for Solar Water Splitting Devices. *J. Am. Chem. Soc.* **2015**, *137*, 4347–4357. [[CrossRef](#)] [[PubMed](#)]
46. Kang, B.K.; Han, G.S.; Baek, J.H.; Lee, D.G.; Song, Y.H.; Kwon, S.B.; Cho, I.S.; Jung, H.S.; Yoon, D.H. Nanodome Structured BiVO₄/GaOxN_{1-x} Photoanode for Solar Water Oxidation. *Adv. Mater. Interfaces* **2017**, *4*, 1–8. [[CrossRef](#)]
47. Liu, X.; Sun, Z.; Cui, S.; Du, P. Cuprous oxide thin film directly electrodeposited from a simple copper salt on conductive electrode for efficient oxygen evolution reaction. *Electrochim. Acta* **2016**, *187*, 381–388. [[CrossRef](#)]